Check for updates

Dynamic response of large tilt-angle flexoelectro-optic liquid crystal modulators

JULIAN A. J. FELLS,[1,4] CHRIS WELCH,[2] WING C. YIP,[3] STEVE J. ELSTON,[1] MARTIN J. BOOTH,[1] GEORG H. MEHL,[2] TIMOTHY D. WILKINSON,[3] AND STEPHEN M. MORRIS[1,5]

[1]*Department of Engineering Science, University of Oxford, Parks Road, Oxford OX1 3PJ, UK*
[2]*Department of Chemistry, University of Hull, Hull HU6 7RX, UK*
[3]*Centre of Molecular Materials for Photonics and Electronics, Electrical Engineering Division, Department of Engineering, University of Cambridge, 9 JJ Thomson Avenue, Cambridge CB3 0FA, UK*
[4]*julian.fells@eng.ox.ac.uk*
[5]*stephen.morris@eng.ox.ac.uk*

Abstract: We present here the first time-resolved tilt-angle and retardance measurements for large-tilt (>45°) flexoelectro-optic liquid crystal modulators. These devices have potential for next generation fast switching (>1 kHz), 0-2π analog phase spatial light modulators (SLMs), with applications in optical beamsteering, microscopy and micromachining. The chiral nematic device used consisted of a mixture of CBC7CB and the chiral dopant R5011 in a nominally 5 μm-thick cell, aligned in the uniform lying helix mode. As the device is dynamically switched over angles of ± 54°, retardance changes of up to 0.17λ are observed. Furthermore, the time-resolved measurements reveal an asymmetry in the tilt in the optic-axis depending on the polarity of the applied electric field. The change in the optic-axis exhibits a pattern dependence, whereby it is determined by both the pulse history and the applied field. This pattern dependence results in tilt-angle errors of up to 8.8°, which could manifest as phase errors as large as 35.2° in potential SLMs. These time domain measurements may allow correction of these deterministic errors, to realize practical devices.

1. Introduction

Flexoelectro-optic Liquid Crystal (LC) modulators [1,2] have enormous potential for a range of applications as their optical properties may be modulated with very fast response times down to less than 100 μs [3]. They can be used in different configurations to modulate polarization, intensity or phase with analog precision. Furthermore, they are an enabling technology for ultrafast (>1 kHz) analog spatial light modulators (SLMs) [4–6]. Analog SLMs allow a beam wavefront to be modulated in two dimensions, and have many diverse applications. For example, by applying modulo 2π phase ramps, they can be used for optical beamsteering, as required for light detection and ranging (LiDAR). They can also be used to correct for optical aberration when focusing through material interfaces, such as in microscopy and for laser micromachining. However, existing commercially available *analog* phase SLMs are restricted to frame rates of ~400 Hz. The ability to increase this frame rate would enhance the performance of existing systems, as well as open up new opportunities. For example, it would allow faster scanning LiDAR, better imaging of live tissue samples, and higher throughput laser micromachining.

Fast flexoelectro-optic switching requires short-pitch chiral nematic LC devices that are subjected to an electric field perpendicular to their helical axis. The flexoelectro-optic effect has been extensively studied [7–12] in order to understand the switching phenomenon and the role of dielectric anisotropy. Of particular interest is the uniform lying helix (ULH) texture

[4], in which the helix axis is aligned parallel to the electrodes and perpendicular to the direction of propagation of the optical beam. The LC material in these devices behaves like an optical waveplate, with an optic-axis which changes (tilts) in response to an applied electric field. This polarization modulation can be converted to a phase modulation by combining it with two quarter waveplates and a polarizer in a reflective configuration [6], to impart a phase change equal to $4 \times$ the tilt-angle.

In order to achieve a full 2π phase modulation range in flexoelectro-optic SLMs, very large tilt-angles of $\pm 45°$ are needed [6,13]. To enhance the flexoelectro-optic effect there has been considerable research on new LC materials [3,10,14–16]. Recently, chiral nematic mixtures consisting of the compound, CBC7CB, have shown tilt angles of up to 72.4° [17]. However, to date, characterization of these large tilt materials has been restricted to measurements of the intensity response when placed between crossed polarizers and subjected to a simple square-wave stimulus. At tilt-angle swings above $\pm 22.5°$, there is a stationary point in the transmission as a function of the applied electric field. To measure wider swings, it is possible to align the optic-axis under zero field with the axis of one of the polarizers [17], but this implicitly assumes that the change in the optic-axis is symmetrical about the zero-field point, which may not be the case. Electric field-induced changes in the birefringence and ionic behavior also add further complications and errors to the measurement. As a result, cross-polarizer intensity-based measurements only yield an average estimate of the tilt-angle. An alternative possibility might be to use a rotating analyzer [18]. However, this method is unsuitable as the device must be switched significantly slower than the mechanically rotating polarizer. At such low switching speeds ionic screening effects dominate the response. Practical devices will require precise control of the tilt-angle and retardance over time and furthermore will be driven with more complex patterns than simple square-wave forms. In this work, we characterize for the first time the dynamic response of large tilt-angle LC flexoelectro-optic modulators, where behavior can be found which cannot be detected using conventional measurement methods. This characterization yields time-resolved measurements of the tilt-angle and retardance which are independent of one another, as well as being independent of changes in device loss.

2. Flexoelectro-optic liquid crystal device

The LC mixture was prepared by dispersing approximately 3 wt% of the chiral dopant R5011 (Merck) with the bimesogen CBC7CB (synthesized in-house) to form a chiral nematic phase. The mixture was capillary filled into a nominally 5 µm-thick glass cell with anti-parallel rubbed polyimide alignment layers and indium tin oxide electrodes. Prior to filling, the cell thickness was measured to be 4.7 µm using white light interference. The cell was mounted on a hot-stage (Linkam LTS350 with TP93 controller) and observed using a polarizing optical microscope (Nikon Photoshot with PixelLink CCD camera). An electric field was applied to the device with an arbitrary function generator (AFG) (Wavetek 195) followed by a $10 \times$ voltage amplifier (FLC Electronics F10AD). Voltages up to $\pm 25V$ were applied (corresponding to an electric field up to ± 5.3 Vµm^{-1}), which allowed $> \pm 45°$ switching without unwinding the helix. The isotropic to chiral nematic phase transition of this mixture was found to occur at 112.7°C on cooling and the chiral nematic phase extended to 97.8°, before the onset of a nematic twist-bend phase. All measurements on the device were carried out at 106°C. Without any field applied, the chiral nematic LC naturally aligned in the Grandjean texture (helix axis perpendicular to the cell surfaces) due to the anchoring conditions. The reflection band was measured using white light interference and was found to lie between 566 nm to 649 nm. The chiral pitch was then estimated to be 374 nm using the wavelengths corresponding to the reflection band and the published values for the ordinary and extraordinary refractive indices of the nematic LC, CBC7CB [19].

Figure 1 shows polarizing optical microscope images for the device in the ULH texture. The LC was aligned in the ULH texture by slowly cooling the device from the isotropic phase

in the presence of a $\pm$ 5.3 Vμm^{-1} 1 kHz square-wave. The temperature was reduced in 1°C increments and held for 10-20 seconds at each temperature. This yielded a 'good' alignment as shown in Fig. 1(a). An applied electric field was required in order to maintain a stable ULH alignment, hence a small residual field of $E = \pm 0.1$V μm^{-1} was used (otherwise the ULH would collapse into a Grandjean or focal conic texture). With an applied electric field of $E = \pm 0.1$V μm^{-1}, there is a contrast of 13.26 between the dark state (i) (aligned with one axis of the crossed polarizers) and the light state (ii) (at 45° to the crossed polarizer axes), from the mean pixel intensities. Images (iii) and (iv) show the device aligned at 22.5° to one of the polarizers for applied electric fields of $E = \pm 0.1$V μm^{-1} and $E = \pm 4.3$V μm^{-1}, respectively. In order to gain some additional insight, an attempt was also made to align the device in a less perfect way, shown in Fig. 1(b). It is not anticipated that the device would be operated under these conditions, but the comparison is useful to better understand the device characteristics. It was difficult to obtain a 'poor' alignment as the LC naturally formed a 'good' alignment. After trial and error, a 'poor' alignment was obtained by cooling from the isotropic phase in the presence of a $\pm$ 2.1 Vμm^{-1} 1 kHz square-wave and applying pressure to the cell with a blunt instrument, shown in Fig. 1(b). With 'poor' alignment, the contrast between the dark state (i) and the light state (ii) is 2.28. Images (iii) and (iv) show the device under 'poor' alignment at 22.5° to one of the polarizer axes, for applied electric fields of $E = \pm 0.1$V μm^{-1} and $E = \pm 4.3$V μm^{-1}, respectively. The ULH alignment was maintained for electric fields up to $E = \pm 5.3$V μm^{-1}, but alignment was lost upon removing the applied electric field.
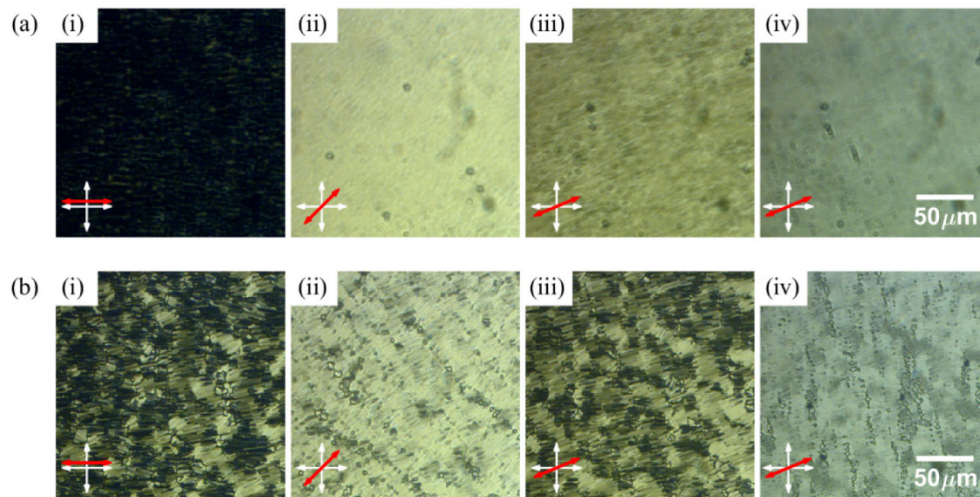
Fig. 1. Microscope images of the liquid crystal device between crossed polarizers under a 1 kHz square-wave electric field, (a) with 'good' alignment, (b) with 'poor' alignment. (i)-(iii) with applied electric field, $E = \pm 0.1$ Vμm^{-1} and orientations of 0°, 45° and 22.5° to the transmission axis of one the polarizers, respectively. (iv) with applied electric field $E = \pm 4.3$ Vμm^{-1} and an orientation of 22.5° to the transmission axis of one the polarizers.

3. Time-resolved measurements

The flexoelectro-optic device was characterized using a recently developed system [20], which provides measurements of the absolute angle of the optic-axis, the retardance change and the optical transmissivity independently of one another over time. Details of the experimental apparatus used to characterize the time-resolved behavior of the flexoelectro-optic switching are provided in detail in [20]. In summary, the technique involves passing circularly polarized light through the sample, followed by a polarizer mounted on a motorized rotation mount and a photodetector. A time-varying electric field is applied to the sample and

the resulting intensity over time is recorded for a range of different static polarizer angles. From this data it is possible to deconvolve the time-varying tilt-angle, retardance and transmissivity of the device, in response to the applied field. By taking measurements using both left circularly and right circularly polarized input light, very high accuracies of $< \pm 0.3°$ tilt-angle error and $< \pm 0.0012\lambda$ retardance are obtained. The system has shown very good agreement with published data for the well-known liquid crystal mixture, E7. The system has also been found to give consistent measurements for different surface alignments [21].
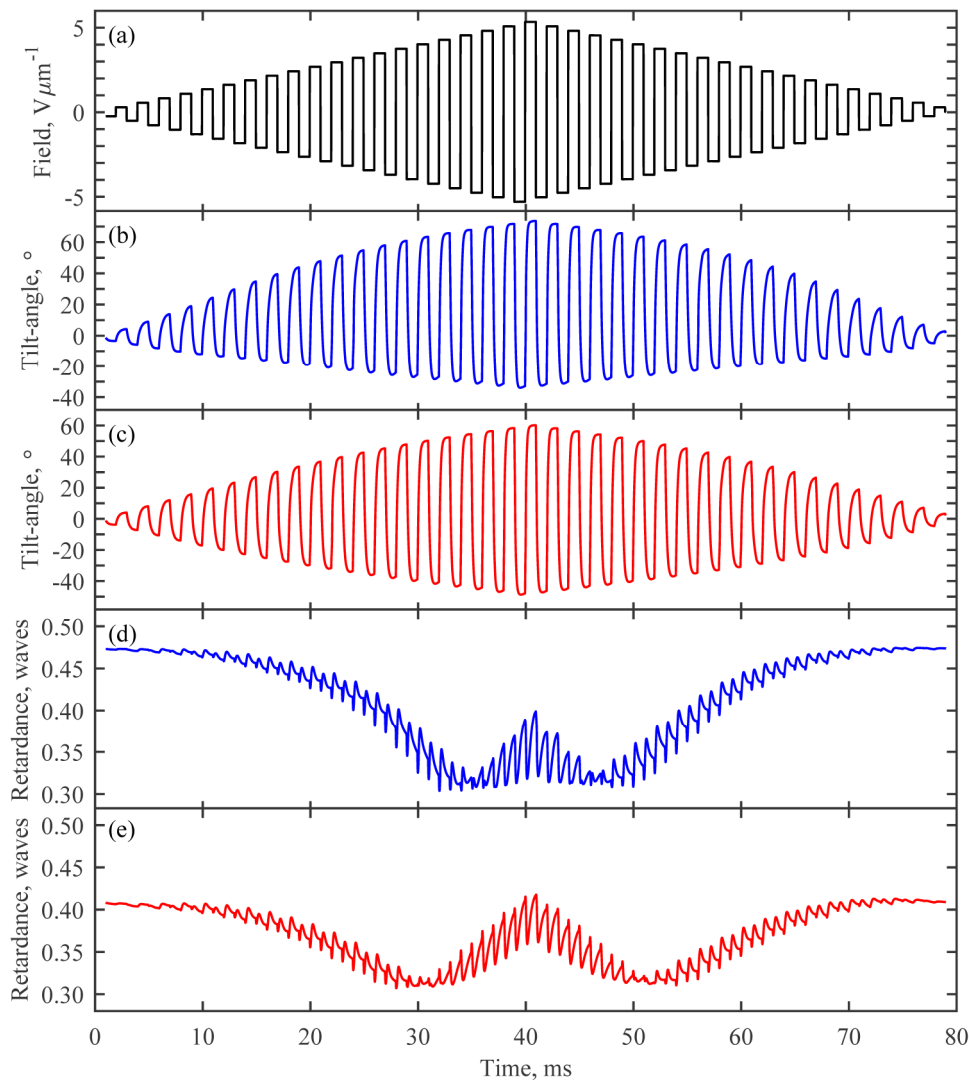
Fig. 2. Time-resolved measurements of the liquid crystal device consisting of the bimesogen, CBC7CB, doped with 3 wt% chiral dopant (R5011) in a 4.7 µm-thick glass cell. (a) input electric field; (b) tilt angle of the optic axis for 'good' alignment; (c) tilt angle of the optic axis for 'poor' alignment; (d) retardance for 'good' alignment; (e) retardance for 'poor' alignment. The underlying data is provided in Data File 1.

For these measurements, the hot-stage supporting the device was transferred between the microscope and the time-resolved measurement system without altering the temperature or removing the electric field. This ensured the LC alignment did not change and the microscope images matched the driving conditions. The AFG was programmed to give a multilevel 1 kHz

pulse pattern which had a series of different concatenated sequences to enable a full characterization from a single measurement. The system generated measurements of the optic-axis angle, retardance and transmissivity over time in response to this stimulus and the full data set is provided in Data File 1.
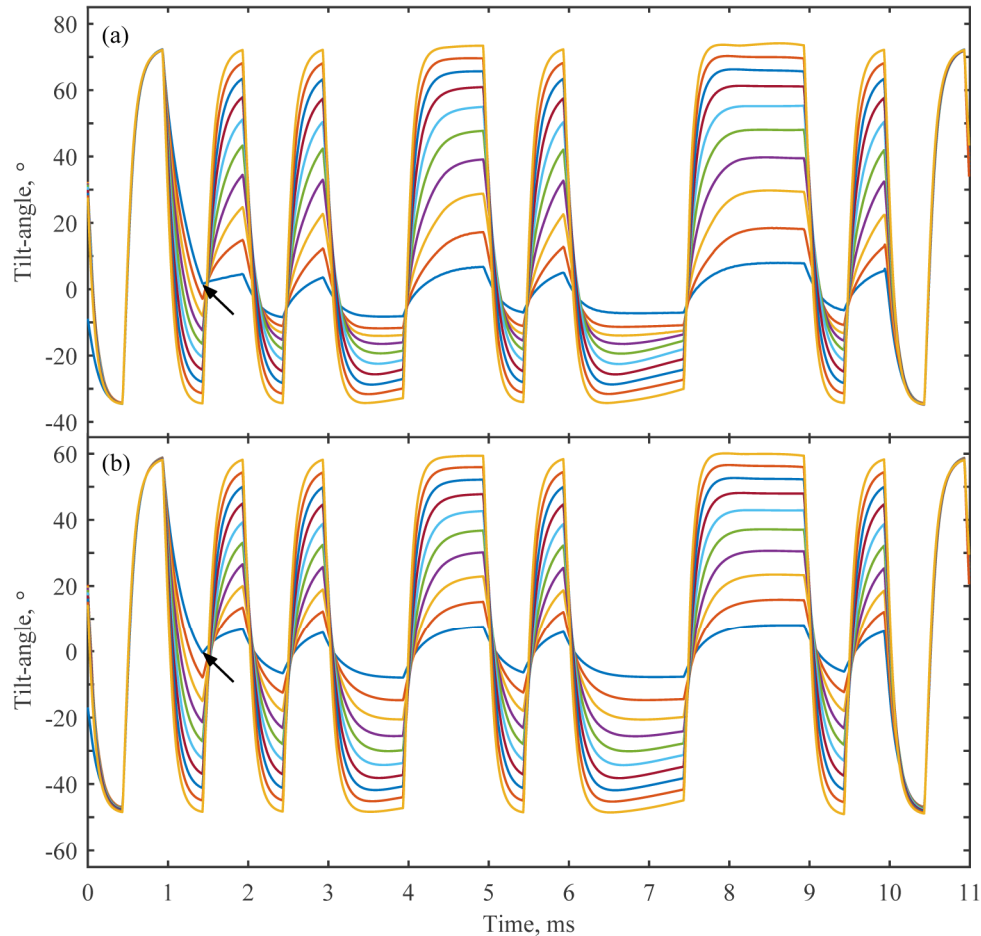
Fig. 3. Time-resolved measurements of the CBC7CB + 3wt% R5011 liquid crystal device, driven by a pattern consisting of the sequence E = {-5.3, 5.3, -x, x, -x, x, -x, -x, x, x, -x, x, -x, -x, -x, x, x, x, -x, x, −5.3, 5.3} Vμm^{-1}, where x is an electric field amplitude that is different for each sequence. Ten sequences with equally-spaced values of x between 0 and 5.3 Vμm^{-1} are overlaid. (a) for the device under 'good' alignment; (b) for the device under 'poor' alignment. The arrows indicate points where the angle of optic-axis is different from subsequent pulses of the same electric field magnitude, as a result of the higher magnitude preceding pulse.

Figure 2 shows time-resolved measurements of the device for a {-x, -x, x, x} repeated sequence where x is a variable electric field magnitude for each repeat, ramping up and down in 20 equally spaced amplitudes up to 5.3 Vμm^{-1}. The electric field applied to the device is shown in Fig. 2(a). The angle of optic-axis measured is shown in Figs. 2(b) and 2(c) for 'good' and 'poor' alignments, respectively. In both cases the downward ramp mirrors the upward ramp, showing that there is no hysteresis. However, there is a marked difference in the tilt-angle symmetry with the polarity of the electrical drive. The device under 'good' alignment shows a very strong asymmetry, extending to positive tilt angles of 73.7° and negative tilt-angles of −34.4°. In contrast, the device with 'poor' alignment shows much less asymmetry, extending to positive angles of 59.7° and negative angles of −49.2°.

The retardance variation over time is shown in Figs. 2(d) and 2(e) for the 'good' alignment and 'poor' alignment, respectively. As expected, the device under 'poor' alignment shows a lower maximum absolute retardance. The retardance changes are found to be 0.17λ for the device with 'good' alignment whereas it is 0.11λ for the device with 'poor' alignment. This change in retardance serves to add to any absolute error in retardance, resulting in unwanted amplitude modulation in phase modulation devices [6].

To explore the pattern dependence, Fig. 3 shows the tilt-angle for a repeated sequence $E = \{-5.3, 5.3, -x, x, -x, x, -x, -x, x, x, -x, x, -x, -x, -x, x, x, x, -x, x, -5.3, 5.3\}$ of electric field in $V\mu m^{-1}$. The repeats are overlaid, for 10 equally-spaced values of x up to 5.3 $V\mu m^{-1}$. Figure 3(a) shows the device under 'good' alignment. Here it can be seen that the rise times are progressively faster as the amplitude of the pulses increases, though single pulses on their own do not appear to reach their maximum value. At longer pulses with high field amplitudes, the tilt-angle reaches a maximum and then reduces slightly over the duration of the pulse. This is the result of an ionic screening effect, whereby charge buildup on the electrodes opposes the driving field, reducing the effective electric field seen across the device. The interplay between rise time and ionic screening results in the maximum tilt-angle occurring at different times within the pulse for different field magnitudes. The asymmetry in the tilt-angle with field polarity observed in Fig. 2 is also evident, with larger tilt magnitudes for the positive polarity. It is also noticeable that the ionic screening effect appears stronger for the negative polarity. Close inspection of the first {-x} (marked with arrows in Fig. 3) shows that it is different to the second {-x} at low electric field values. This is important as it appears that there is a pattern dependence, whereby the tilt-angle is not only dependent on the instantaneous field, but also on preceding pulses. Figure 3(b) shows that the device under 'poor' alignment exhibits similar features to the 'good' alignment case, except that the asymmetry is very much less pronounced.

4. Analysis

The key parameter is the variation in tilt-angle with applied electric field, as this directly translates into either a phase modulation or an intensity modulation. However, any residual change in the retardance is undesirable as it can lead to errors. To characterize the response, the variation in the angle of the optic-axis, the retardance and the rise-time are plotted as a function of applied electric field in Fig. 4. A similar ramp to that used for Fig. 2 was used to obtain the data, except there were 3 successive periods at each field amplitude, to ensure the response had stabilized. By considering each pulse pair of opposite polarity, the overall absolute angle of the optic axis was separated into two components: a half-angle $(\varphi^{+}-\varphi^{-})/2$ and a mean angle $(\varphi^{+} + \varphi^{-})/2$, where φ^{+} and φ^{-}, are the angles of optic axis for the positive and negative electric field pulses, respectively. Figure 4(a) shows the half-angle and mean angle for both 'good' and 'poor' alignment. It can be seen that the half-angle versus field for the two cases overlay each other. The mean angles for the two alignments both increase with field amplitude and saturate above $E = 4$ $V\mu m^{-1}$. However, whilst the device under 'good' alignment shows a change in the mean optic axis of $19.9°$, under 'poor' alignment the mean optic axis shows a $5.6°$ change.

We speculate that the observed differences in the switching behavior are the result of helix realignment that occurs at low electric field strengths and suggest that the change in mean angle is indicative of a change in the effective helix axis angle, which is occurring simultaneously with the change in the half-angle. Above a threshold electric field, there is no further change in effective helix axis angle. The images in Fig. 1 show some change in the structure between $E = 0.1$ to 4.3 $V\mu m^{-1}$. These measurements show that some form of stabilization of the LC structure may be required for practical devices. For example, polymerization [4] or photoalignment [22] may allow the helix-axis to be held in a constant orientation. However, a side-effect of this may be a reduced switching angle [23].

At low values, the tilt-angle, φ, with applied electric field, E, may be approximated by [1,24]

$$\tan\varphi = \frac{(e_1 - e_3)}{(K_{11} + K_{33})}\frac{p}{2\pi}E \qquad (1)$$

where e_1 and e_3 are the splay and bend flexoelectric coefficients respectively, K_{11} and K_{33} are the splay and bend elastic coefficients respectively, and p is the chiral pitch. The flexoelastic ratio $(e_1 - e_3)/(K_{11} + K_{33})$ was estimated to be 4.23 V^{-1}, from the gradient of the half-angle at low electric fields. This compares with 3.67 V^{-1} previously reported [17], though both measurements have uncertainty in the chiral pitch.
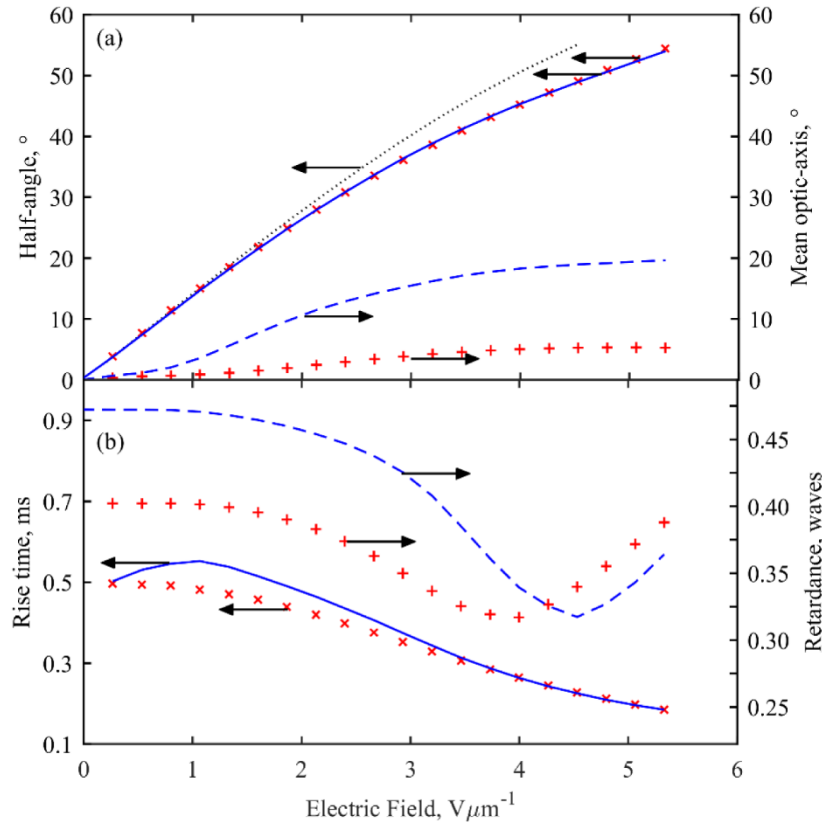
Fig. 4. Device parameters determined from the time-resolved measurements on the CBC7CB + 3wt% R5011 liquid crystal device. (a) The angle of the optic-axis as a function of the applied electric field separated into two components: the flexoelectro-optic half-angle and the mean angle of the optic axis. (— blue) measured half-angle under 'good' alignment; (× red) measured half-angle under 'poor' alignment; (— — blue) mean angle of the optic-axis under 'good' alignment; (+ red) mean angle of optic-axis under 'poor' alignment; (····· black) theoretical prediction of tilt-angle from Eq. (2). (b) The rise time and retardance change. (— blue) rise time under 'good' alignment; (× red) rise time under 'poor' alignment; (— — blue) retardance change under 'good' alignment; (+ red) retardance change under 'poor' alignment.

For large tilt-angles, a constrained-pitch model is required [9,11]

$$\tan\varphi = \frac{(e_1 - e_3)p}{4\pi K_{22}}E - \frac{(K_{11} - 2K_{22} + K_{33})\sin\varphi}{2K_{22}} \qquad (2)$$

where K_{22} is the twist elastic coefficient. Using the extracted value of the flexoelastic coefficient and published values for the splay, twist and bend elastic constants at the same

shifted temperature (K_{11} = 6.6 pN, K_{22} = 1.8 pN and K_{33} = 0.64 pN [19]), the theoretical plot predicted by Eq. (2) is shown in Fig. 4(a). This plot shows a sublinear response similar to the measured data, but overestimates the tilt-angle. This is likely to be due to dielectric coupling as discussed in [25] (the dielectric anisotropy, $\Delta\varepsilon$, of CBC7CB at this shifted temperature is measured to be approximately 2.1 at 5-60 kHz [19]). The critical electric field, E_c, above which the helix unwinds, is given by [26]

$$E_c = \pm \frac{\pi^2}{p}\left(\frac{K_{22}}{\varepsilon_0 \Delta\varepsilon}\right) \tag{3}$$

where ε_0 is the permittivity of free space. This corresponds to a critical electric field of 7.8 Vμm^{-1}, so the maximum applied field of ± 5.3 Vμm^{-1} is well within the limit before the helix unwinds.

Figure 4(b) shows the rise time and the retardance for the two alignments. The rise time is the 10-90% switching time from the negative angle to the positive angle. Previously reported response times appear shorter because they are indirectly measured as the 10-90% change in intensity between zero field and a maximum field, which would be less than half the full swing considered here. The response times are broadly similar for both alignments and decrease with field magnitude to times as short as 185 μs. The retardance under 'good' alignment is higher than that under 'poor' alignment, as expected, and the retardance decreases with field magnitude up to 4.3 Vμm^{-1}.

5. Pseudo-random modulation

In use, more random electric field patterns will be applied, so a pattern of the repeating sequence {-x, -x, x, x}, where x is a pseudo-random electric field (of either polarity) between E = −5.3 Vμm^{-1} and E = 5.3 Vμm^{-1}, was tested. This ensured that the rise-time did not limit the performance and the polarity of the electric field was balanced to mitigate ionic screening effects. Figure 5 shows the angle of optic-axis with time, along with the predicted angle, from the tilt-angle versus field characteristics presented in Fig. 4 (taking into account the asymmetry caused by the change in mean angle). Also shown are errors (taken at the end of the pulse to allow settling) where they exceed 3°. The errors are up to 8.8° with 'good' alignment and 3.4° with 'poor' alignment, as shown in Figs. 5(a) and 5(b), respectively. Whilst these seem small, in a full phase modulator implementation, the phase change is equal to 4 × the tilt-angle [6,13], so this could translate into problematic phase errors of up to 35.2°.

The larger error for the 'good alignment' is likely due to the pattern dependent error when there is a large difference in the electric field between consecutive pulses, illustrated by the arrows in Fig. 3. The 'good' alignment case has a larger change in mean angle of optic axis and therefore larger differences in electric field between consecutive pulses. Although the errors are pattern dependent they are deterministic and repeatable, opening up the possibility of correcting for them digitally in software. The rise time as a function of applied field has been measured, so this could be used to determine the error associated with the finite rise time and compensate for it. The decay associated with ionic screening could be characterized for different electric fields, enabling that error to be compensated. The pattern dependent error could also be characterized for various field increments between consecutive pulses, enabling this error to be reduced.
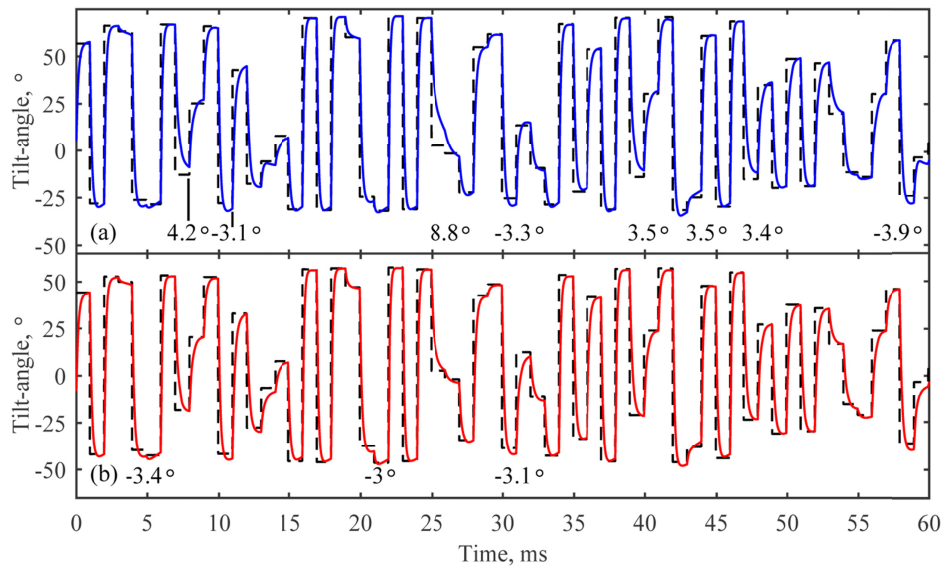
Fig. 5. The flexoelectro-optic tilt-angle over time for the CBC7CB + 3wt% R5011 liquid crystal device when subjected to a pseudo-random waveform pattern. The pattern consists of a repeated sequence {-x, -x, x, x}, where x is pseudo-random. (a) for the device under 'good' alignment; (b) for the device under 'poor' alignment. (—) Measured angle of the optic axis; (- -) Predicted angle of optic axis, taking into account the asymmetry in the tilt-angle versus electric field. Errors between the measured angle and the predicted angle (taken at the end of each pulse) greater than 3° are labelled below the relevant pulse.

6. Conclusions

This work has reported the dynamic properties of large tilt-angle flexoelectro-optic modulators for the first time. Our system provides accurate and independent measurements of tilt-angle and retardance, even for tilt-angles that are greater than ± 45°. The system is robust to simultaneous changes in tilt-angle, retardance and loss. We show that the angle of optic-axis depends not only on the applied electric field, but also on the pattern of preceding pulses. This indicates that some form of LC stabilization may be required. The results reveal differences in the switching behavior of large tilt-angle devices that are not readily detectable using conventional intensity modulation-based measurements. Tests with a pseudo-random sequence show that pattern dependent tilt-angle errors of up to 8.8° are observed which would lead to phase modulation errors of up to 35.2°. These deterministic errors may be corrected for by calibrating devices using the techniques presented in this work. We believe that these time-resolved measurements of large tilt-angle materials will therefore become important for characterizing and calibrating future flexoelectro-optic spatial light modulators for a multitude of applications.

The underlying data supporting this work is provided in Data File 1.

Funding

References

1. J. S. Patel and R. B. Meyer, "Flexoelectric electro-optics of a cholesteric liquid crystal," Phys. Rev. Lett. **58**(15), 1538–1540 (1987).
2. J. S. Patel and S. Lee, "Fast linear electro-optic effect based on cholesteric liquid crystals," J. Appl. Phys. **66**(4), 1879–1881 (1989).

3. S. M. Morris, M. J. Clarke, A. E. Blatch, and H. J. Coles, "Structure-flexoelastic properties of bimesogenic liquid crystals," Phys. Rev. E Stat. Nonlin. Soft Matter Phys. **75**(4), 041701 (2007).
4. P. Rudquist, L. Komitov, and S. T. Lagerwall, "Volume-stabilized ULH structure for the flexoelectro-optic effect and the phase-shift effect in cholesterics," Liq. Cryst. **24**(3), 329–334 (1998).
5. J. Chen, S. M. Morris, T. D. Wilkinson, J. P. Freeman, and H. J. Coles, "High speed liquid crystal over silicon display based on the flexoelectro-optic effect," Opt. Express **17**(9), 7130–7137 (2009).
6. J. A. J. Fells, X. Wang, S. J. Elston, C. Welch, G. H. Mehl, M. J. Booth, S. M. Morris, M. J. Booth, and S. M. Morris, "Flexoelectro-optic liquid crystal analog phase-only modulator with a 2π range and 1 kHz switching," Opt. Lett. **43**(18), 4362–4365 (2018).
7. P. Rudquist, M. Buivydas, L. Komitov, and S. T. Lagerwall, "Linear electro-optic effect based on flexoelectricity in a cholesteric with sign change of dielectric anisotropy," J. Appl. Phys. **76**(12), 7778–7783 (1994).
8. P. Rudquist, L. Komitov, and S. T. Lagerwall, "Linear electro-optic effect in a cholesteric liquid crystal," Phys. Rev. E Stat. Phys. Plasmas Fluids Relat. Interdiscip. Topics **50**(6), 4735–4743 (1994).
9. P. Rudquist, T. Carlsson, L. Komitov, and S. T. Lagerwall, "The flexoelectro-optic effect in cholesterics," Liq. Cryst. **22**(4), 445–449 (1997).
10. H. J. Coles, M. J. Clarke, S. M. Morris, B. J. Broughton, and A. E. Blatch, "Strong flexoelectric behavior in bimesogenic liquid crystals," J. Appl. Phys. **99**(3), 034104 (2006).
11. S. D. Lee, J. S. Patel, and R. B. Meyer, "Effect of flexoelectric coupling on helix distortions in cholesteric liquid crystals," J. Appl. Phys. **67**(3), 1293–1297 (1990).
12. D. R. Corbett and S. J. Elston, "Modeling the helical flexoelectro-optic effect," Phys. Rev. E Stat. Nonlin. Soft Matter Phys. **84**(4), 041706 (2011).
13. J. E. Stockley, G. D. Sharp, S. A. Serati, and K. M. Johnson, "Analog optical phase modulator based on chiral smectic and polymer cholesteric liquid crystals," Opt. Lett. **20**(23), 2441 (1995).
14. K. L. Atkinson, S. M. Morris, F. Castles, M. M. Qasim, D. J. Gardiner, and H. J. Coles, "Flexoelectric and elastic coefficients of odd and even homologous bimesogens," Phys. Rev. E Stat. Nonlin. Soft Matter Phys. **85**(1), 012701 (2012).
15. K. L. Atkinson, S. M. Morris, M. M. Qasim, F. Castles, D. J. Gardiner, P. J. W. Hands, S. S. Choi, W. S. Kim, and H. J. Coles, "Increasing the flexoelastic ratio of liquid crystals using highly fluorinated ester-linked bimesogens," Phys. Chem. Chem. Phys. **14**(47), 16377–16385 (2012).
16. A. Varanytsia and L.-C. Chien, "Bimesogen-enhanced flexoelectro-optic behavior of polymer stabilized cholesteric liquid crystal," J. Appl. Phys. **119**(1), 014502 (2016).
17. A. Varanytsia and L.-C. Chien, "Giant Flexoelectro-optic Effect with Liquid Crystal Dimer CB7CB," Sci. Rep. **7**(1), 41333 (2017).
18. I. Wood and A. Glazer, "Ferroelastic phase transition in BiVO4 I. Birefringence measurements using the rotating-analyser method," J. Appl. Cryst. **13**(3), 217–223 (1980).
19. G. Babakhanova, Z. Parsouzi, S. Paladugu, H. Wang, Y. A. Nastishin, S. V. Shiyanovskii, S. Sprunt, and O. D. Lavrentovich, "Elastic and viscous properties of the nematic dimer CB7CB," Phys. Rev. E **96**(6), 062704 (2017).
20. J. A. J. Fells, S. J. Elston, M. J. Booth, and S. M. Morris, "Time-resolved retardance and optic-axis angle measurement system for characterization of flexoelectro-optic liquid crystal and other birefringent devices," Opt. Express **26**(5), 6126–6142 (2018).
21. J. J. Sandford O'Neill, J. A. J. Fells, C. Welch, G. Mehl, W. C. Yip, T. D. Wilkinson, M. J. Booth, S. J. Elston, and S. M. Morris, "Robust measurement of flexoelectro-optic switching with different surface alignments," J. Appl. Phys. **125**(9), 093104 (2019).
22. W. M. Gibbons, P. J. Shannon, S.-T. Sun, and B. J. Swetlin, "Surface-mediated alignment of nematic liquid crystals with polarized laser light," Nature **351**(6321), 50 (1991).
23. B. J. Broughton, M. J. Clarke, S. M. Morris, A. E. Blatch, and H. J. Coles, "Effect of polymer concentration on stabilized large-tilt-angle flexoelectro-optic switching," J. Appl. Phys. **99**(2), 023511 (2006).
24. I. Dierking, P. Rudquist, L. Komitov, S. T. Lagerwall, and B. Stebler, "Investigations on the flexoelectric and electroclinic effect in a cholesteric phase with twist inversion," Mol. Cryst. Liq. Cryst. (Phila. Pa.) **304**(1), 389–402 (1997).
25. F. Castles, S. M. Morris, and H. J. Coles, "Flexoelectro-optic properties of chiral nematic liquid crystals in the uniform standing helix configuration," Phys. Rev. E Stat. Nonlin. Soft Matter Phys. **80**(3), 031709 (2009).
26. P. G. de Gennes, J. Prost, The Physics of Liquid Crystals, (Clarendon Press, 1995).